Astron. Astrophys. 245, 129–135 (1991)

ASTRONOMY AND ASTROPHYSICS

Nonlinear nonaxisymmetric dynamo models for cool stars

D. Moss[1], I. Tuominen[2], and A. Brandenburg[2,⋆]

[1] Mathematics Department, The University, Manchester, M13 9PL, UK
[2] Observatory and Astrophysics Laboratory, Tähtitorninmäki, SF-00130 Helsinki, Finland

Received August 6, accepted October 20, 1990

Abstract. Observational evidence for long-lived nonaxisymmetric features on the surfaces of rapidly rotating late-type giant stars (e.g. FK Comae and RS CVn stars) is beginning to be found. By analogy with sunspots, these features may be associated with large scale nonaxisymmetric magnetic field structures, generated by a dynamo operating in the convective envelopes. We describe a nonlinear nonaxisymmetric dynamo model, and show that for a simple 'α-quenching' nonlinearity together with suitable choices of underlying radial profiles of differential rotation and the α-effect, stable nonaxisymmetric solutions can be found by numerical integration.

Key words: mean-field dynamos – nonaxisymmetric magnetic fields – stellar magnetic fields – active giant stars

1. Introduction

Traditionally the prime objective of astrophysical dynamo theory has been to understand the solar cycle. This is very reasonable, given that there is an abundance of observations of the solar surface field and associated phenomena, extending over hundreds of years. In addition, information about the internal solar differential rotation is now becoming available. In contrast, for other cool stars that are candidates for having fields generated by a contemporary dynamo we have generally only very coarse grained, whole disk, information about proxies for field cycles, extending at best over a couple of decades.

Dynamo theorists have largely studied axisymmetric models, for very good reasons. The mean solar field appears to be predominantly axisymmetric (although there are hints, from the "sectorial structure" that weak nonaxisymmetric components may be present); and in simple mean field dynamos the most readily excited modes are often axisymmetric. Although linear kinematic models that are strictly axisymmetric and in which the driving mechanisms of dynamo action (usually α-effect and differential rotation) are prescribed can reproduce quite successfully the observed features of the solar cycle, more realistic models that determine these effects self-consistently, by solving simultaneously the full magnetohydrodynamical, dynamical and thermal equations, are much less satisfactory. Indeed, it is clear that there is still much to be learned about the effects of even idealized nonlinearities in the axisymmetric mean field dynamo equations (e.g. Brandenburg et al. 1989a (henceforth BKMMT) and 1989b).

Recently the detection of indicators of surface structure has been reported on a few late type stars that are expected to possess extensive convective envelopes. For example, Piskunov et al. (1990) have used surface imaging techniques to produce maps showing large-scale nonaxisymmetric surface temperature inhomogeneities on the "active giant" HD32918. These "cool spots" seem to define an "active longitude". By analogy with sunspots, this may be evidence for the presence of a predominantly nonaxisymmetric magnetic field. Jetsu et al. (1990) have found a 2.8 yr variation in the amplitude of the photometric rotation modulation, superimposed on a 9 yr cycle in the mean brightness, for the FK Comae star HD199178. The persistence of the phase coherence over 13 years suggests the possibility of a long-lived nonaxisymmetric surface component of magnetic field.

BKMMT demonstrates, for the case of strict axisymmetry, that linear dynamo models are of limited usefulness in predicting the final field configurations for supercritical dynamo parameters. The same appears likely to be true also for nonaxisymmetric configurations. Rädler et al. (1990; henceforth RWBMT) have already made numerical investigations of the time evolution of nonlinear (α-quenched) mean field dynamo models. Their work reveals quite complex behaviour, even in the limited parameter space investigated. For some models nonaxisymmetric modes are stable, and there is even a model with a "mixed" solution, with axi- and nonaxisymmetric components both present.

The present paper describes a new, independent computer code to solve, in three spatial dimensions, the same time dependent, quasi-kinematic, nonlinear mean field dynamo equation as studied by RWBMT, although the numerical algorithm is quite different from that of RWBMT. It would be relatively straightforward to adapt the code to include other types of nonlinearity than α-quenching, although this has not yet been attempted. The new code has been written for and implemented on a vector processor, and so is substantially faster than that of RWBMT. (A single time step at the standard resolution $NI=31$, $NJ=61$, $N=3$ – see Sect. 2 – takes ca. 0.033 s on an Amdahl VP1200.) Thus a more extensive survey of parameter space at higher spatial resolution has been possible. However the notation and general philosophy of this paper is generally consistent with that of RWBMT, and many of their introductory and concluding remarks are relevant here also.

Send offprint requests to: D. Moss

⋆ Present address: Nordita, Blegdamsveg 17, DK-2100, Copenhagen, Denmark

2. The model

We solve the standard mean field dynamo equation

$$\frac{\partial \boldsymbol{B}}{\partial t}=\nabla\times(\boldsymbol{u}\times\boldsymbol{B}+\alpha\boldsymbol{B})-\nabla\times\eta\nabla\times\boldsymbol{B}, \tag{1}$$

in the spherical volume $0\le r\le R$. r, θ, λ are spherical polar coordinates with axis the rotation axis. We make the simplifying assumptions that $\boldsymbol{u}=\boldsymbol{\Omega}\times\boldsymbol{r}$, where $\boldsymbol{\Omega}=\Omega(r)\boldsymbol{k}$ is a prescribed differential rotation ($\boldsymbol{k}$ a unit vector) and that η is a constant (turbulent) resistivity. With the scalings

$$\tau=R^2\eta^{-1}t, \quad x=R^{-1}r, \quad \Omega=\bar{\Omega}\tilde{\Omega}, \quad \alpha=\bar{\alpha}\tilde{\alpha}$$

Eq. (1) becomes

$$\frac{\partial \boldsymbol{B}}{\partial \tau}=\nabla\times(C_\omega\tilde{\Omega}(\boldsymbol{k}\times\hat{\boldsymbol{r}}x)\times\boldsymbol{B}+C_\alpha\tilde{\alpha}\boldsymbol{B})-\nabla\times\nabla\times\boldsymbol{B} \tag{2}$$

where

$$C_\alpha=\frac{R\bar{\alpha}}{\eta}, \quad C_\omega=\frac{R^2\bar{\Omega}}{\eta},$$

are the usual dynamo parameters and $\bar{\alpha}$ and $\bar{\Omega}$ are typical values of α and Ω. We choose to write

$$\tilde{\alpha}=\alpha_0(x,\boldsymbol{B})\cos\theta. \tag{3}$$

For strictly linear calculations $\alpha_0=f(x)$, where $f(x)$ is a prescribed function. For the nonlinear calculations we adopt

$$\alpha_0=\frac{f(x)}{1+\boldsymbol{B}^2(r,\theta,\lambda)}, \tag{4}$$

representing a simple "α-quenching" mechanism driven by the interaction of the magnetic field with the turbulence (e.g. Rüdiger 1973). We perform some computations with "uniform" source profiles, when

$$\tilde{\Omega}=-x, \quad f(x)=1.$$

Otherwise we use

$$f(x)=\begin{cases}\dfrac{15}{16d_\alpha}(1-\xi_\alpha^2)^2, & |\xi_\alpha|<1,\\ 0, & |\xi_\alpha|>1,\end{cases} \tag{5}$$

$$\tilde{\Omega}(x)=\begin{cases}-1, & \xi_\omega\le -1\\ -\dfrac{1}{2}\left(1-\dfrac{3}{2}\xi_\omega+\dfrac{1}{2}\xi_\omega^3\right), & |\xi_\omega|<1\\ 0, & \xi_\omega>1,\end{cases} \tag{6}$$

where $\xi_\alpha=(x-x_\alpha)/d_\alpha$ and $\xi_\omega=(x-x_\omega)/d_\omega$. These profiles have the same spatial structure as those used by RWBMT and are determined by the four parameters x_α, x_ω, d_α, d_ω.

We split the magnetic field into poloidal and toroidal parts, $\boldsymbol{B}=\boldsymbol{B}_{\rm p}+\boldsymbol{B}_{\rm T}$, and write

$$\boldsymbol{B}_{\rm p}=\nabla\times(a(x,\theta)\hat{\boldsymbol{\lambda}})+\nabla\times\nabla\times(\Phi(x,\theta,\lambda)\hat{\boldsymbol{r}}),$$

$$\boldsymbol{B}_{\rm T}=b(x,\theta)\hat{\boldsymbol{\lambda}}+\nabla\times(\Psi(x,\theta,\lambda)\hat{\boldsymbol{r}}),$$

(cf. Chandrasekhar 1961). We then expand

$$\Phi=\sum_{m=1}^{N}\Phi_m(x,\theta)e^{im\lambda},$$

$$\Psi=\sum_{m=1}^{N}\Psi_m(x,\theta)e^{im\lambda}.$$

The radial component of Eq. (1) and the radial component of its curl yield a set of quasi-parabolic partial differential equations for a, b, $L\Phi_m$ and $L\Psi_m$, $m=1,\ldots,N$, (cf. Stix 1971) where

$$L\equiv\frac{\partial^2}{\partial\theta^2}+\cot\theta\frac{\partial}{\partial\theta}-m^2\operatorname{cosec}^2\theta.$$

Given current values of Φ_m, Ψ_m, the advanced values of $L\Phi_m$, $L\Psi_m$ can be obtained by integrating these partial differential equations on a x, θ grid. We use a Dufort-Frankel type method. Φ_m, Ψ_m can then be recovered at the advanced time. After each step the function $\alpha\boldsymbol{B}=\boldsymbol{g}$ (r,θ,λ) is expanded in the form

$$\boldsymbol{g}(r,\theta,\lambda)=\sum_{m=0}^{M}\boldsymbol{g}_m(r,\theta)e^{im\lambda}$$

using fast Fourier transforms, and the functions $\boldsymbol{g}_m$ are used to calculate the terms arising from $\nabla\times(\alpha\boldsymbol{B})$ on the right hand side of Eq. (1).

The equations were solved over $0\le x\le 1$, $0\le\theta\le\pi$, with boundary condition at $x=1$ that $\boldsymbol{B}$ fits smoothly on to a curl-free external field. The condition on the poloidal field components was imposed by an extension of the matrix method used in BKMMT. NI points were uniformly distributed in radius and NJ in θ with, typically, $NI=31$, $NJ=61$; usually $N=3$. Some solutions were confirmed at spatial resolutions of 41×81 or 51×101, and also with $N=5$. Typical timesteps were $\Delta\tau=2.5\,10^{-5}$ or $5\,10^{-5}$.

To interpret the results it is convenient to define the quantities $E^{(\rm S)}$ and $E^{(\rm A)}$, the energies in the region $r\le R$ of the parts of the field that are respectively symmetric and antisymmetric with respect to the rotational equator. We then introduce the overall parity parameter

$$P=\frac{E^{(\rm S)}-E^{(\rm A)}}{E^{(\rm S)}+E^{(\rm A)}},$$

where $-1\le P\le 1$ (cf. BKMMT). It is useful also to define the total energies in each Fourier component of field, E_m, and the corresponding parity parameters for each mode, P_m, $m=0,1,\ldots,N$. A measure of the degree of axisymmetry of the field is given by

$$M=1-E_0/E,$$

(cf. RWBMT) where $E=E^{(\rm S)}+E^{(\rm A)}$ is the total magnetic energy in the sphere $r\le R$. $M=0$ for a purely axisymmetric field and $M=1$ for a field with no $m=0$ component. We also use the notation, introduced by RWBMT, whereby **A1** denotes a solution that is a mixture of $A1$, $A3$, $A5$, ... modes, and **S1** a solution that consist of $S1$, $S3$, $S5$, ... modes. Similarly **S0** and **A0** denote axisymmetric field configurations with $P=\pm 1$ respectively.

When describing and interpreting the results we distinguish between limit cycles where the energies in the various modes oscillate regularly, and steady solutions where the energies E_m are constant, although the fields themselves may only appear steady when viewed in a suitable rotating frame.

In Sect. 4.1 we describe some numerical comparisons between our code and that of RWBMT for α^2 dynamos ($C_\omega=0$). We did not attempt to reproduce the periodic mixed parity nonaxisymmetric solution found by RWBMT as the α and Ω-profiles for that

model are so spatially localized that they cannot adequately be represented by our relatively coarse spatial grid.

3. Linear results

As the result of some experimentation we studied the three profiles, U, D, and E, defined by the parameters given in Table 1. Marginal values of C_α for excitation of selected modes for these profiles are presented in Table 2. These results were determined by an eigenvalue calculation using finite differences in the radial direction together with a truncated expansion in spherical harmonics. Relatively small values of C_ω were considered, in order that the nonaxisymmetric modes were not too severely inhibited by a strong differential rotation. Interpolations on test computations with our nonlinear code, suppressing the nonlinearity in α, show reasonable agreement with the results of the linear code. Our feeling was that nonlinear axisymmetric modes are more likely to persist if the marginal dynamo numbers of the nonaxisymmetric modes are not significantly smaller than those of axisymmetric modes, although it is certainly not true that the nonlinear behaviour at supercritical C_α can be predicted from a knowledge of the positions of the linear theory bifurcations (see, e.g. BKMMT). From Table 2 it appears that this condition is marginally satisfied for the uniform profile U at $C_\omega = 0$. We are primarily interested in oscillatory solutions, which for an isotropic α-effect (α a scalar) means we need $C_\omega \neq 0$. Thus profiles D and E seemed more promising. In particular, for profile E at modest values of C_α there is a comparatively large range of C_ω in which the marginal dynamo numbers of the nonaxisymmetric modes are smaller than those of the axisymmetric modes.

Table 1. Parameter values for the source profiles investigated

Profile	x_α	d_α	x_ω	d_ω
U	Uniform profiles			
D	0.75	0.25	0.75	0.25
E	0.75	0.25	0.50	0.25

Table 2. Approximate critical values of C_α for excitation of various linear modes. A zero in the frequency column indicates a steady mode. The lowest value of $C_{\alpha c}$ for each angular velocity distribution is shown in bold type

Profile	C_ω	Mode	$C_{\alpha c}$	Frequency
U	0	A0	**7.6**	0
		S0	7.8	0
		A1	8.0	0.9
		S1	7.7	2.2
	−300	A0	**9.5**	29
		S0	10.4	26
		A1	15.2	212
		S1	15.2	212
D	−100	A0	**4.0**	28
		S0	4.1	27
		A1	4.7	78
		S1	4.6	79
E	−100	A0	3.79	0
		S0	3.74	0
		A1	3.74	2.1
		S1	**3.70**	2.1
	−150	A0	3.97	0
		S0	3.88	5.6
		A1	3.79	1.2
		S1	**3.75**	1.3
	−300	A0	4.14	25.5
		S0	4.20	18.5
		A1	3.85	−1.9
		S1	**3.81**	−1.5

4. Nonlinear results

4.1. Uniform α-profile, $C_\omega = 0.0$

A preliminary set of computations were performed with the uniform profile $f = 1$, and $\Omega = 0.0$. α-quenching, as prescribed by Eq. (4), provided the only nonlinearity. We studied the case $C_\alpha = 10.0$, a clearly supercritical value. Our results are consistent with those of RWBMT. The only solution stable to both axisymmetric and nonaxisymmetric perturbations is the $A0$ solution ($P = -1.0$, $M = 0.0$). The $S0$ solution, when slightly perturbed, evolves towards this solution via a circuitous path in the P/M diagram, that passes close to $P = 1.0$, $M = 1.0$ before moving along the diagonal joining (1.0, 1.0) and (−1.0, 0.0). Evolution near (1.0, 1.0) is very slow. Computations started from arbitrary points in the P/M plane also eventually evolve to (−1.0, 0.0) along this diagonal, in much the same manner as described by RWBMT. A more detailed comparison of the two codes showed that the structures of the fields at a given point of the diagonal locus of slowly evolving solutions are very similar and the energies agree to within about 10%. It is difficult to compare the effective resolutions of our grid point method (for r and θ) with the spectral code of RWBMT, but this agreement would seem to be fairly satisfactory. We did find it more difficult to reproduce the detailed initial evolution from an arbitrary field configuration towards this diagonal in the P/M plane. The explanation would appear to be that this initial evolution is relatively rapid and depends sensitively on both the detailed configuration of the initial fields and perhaps on the "start up" procedure employed for the first time step.

4.2. Uniform profiles with differential rotation

We performed a few exploratory calculations with uniform α and Ω-profiles. Bearing in mind the inhibition of nonaxisymmetric modes by strong differential rotation in linear theory we restricted our calculations to $C_\omega = -300$. Table 2 shows that, even with this relatively modest value of C_ω, the axisymmetric modes are now excited at significantly smaller values than the nonaxisymmetric. We found that with, for example, $C_\alpha = 30$ the field evolves on a global diffusion timescale to an A0 configuration. This result is typical.

4.3. Profile D

Bearing in mind the linear results shown in Table 1, for our investigations we chose $C_\omega = -100$ and allowed C_α to vary. We

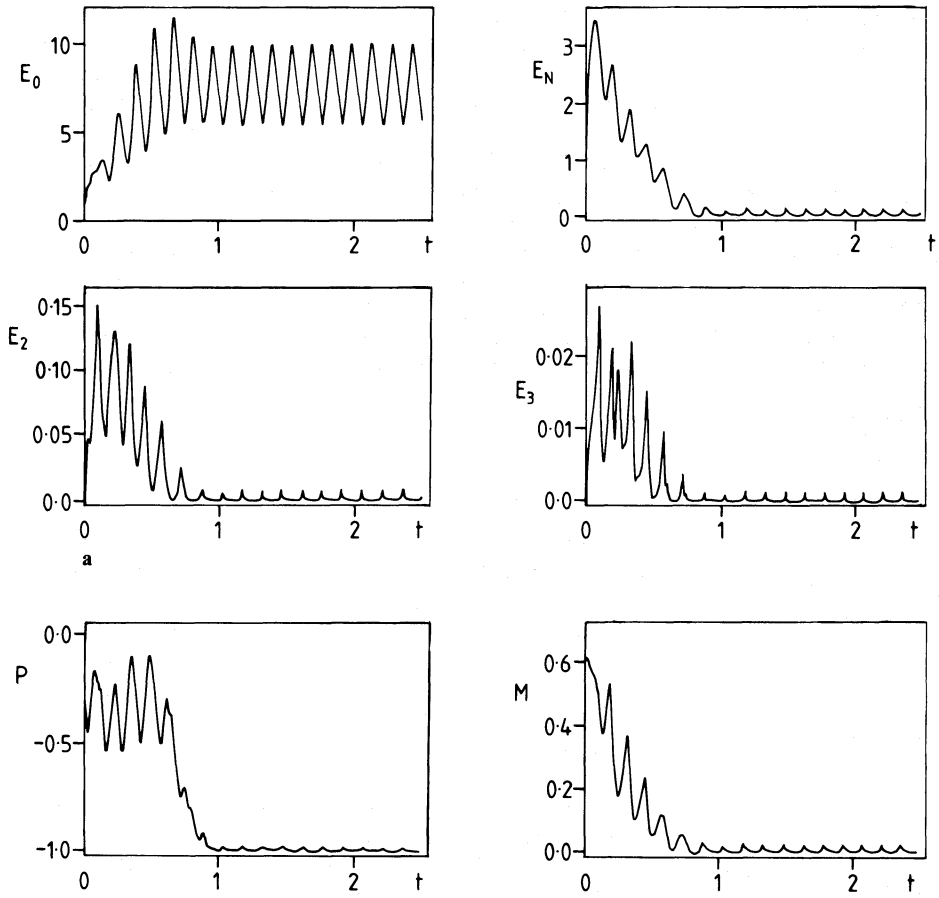

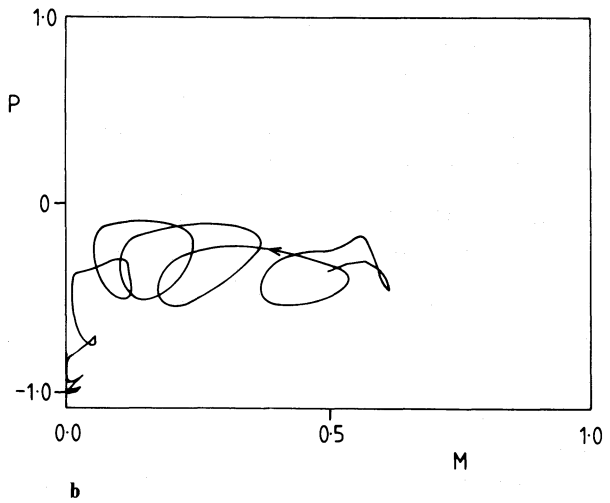

Fig. 1a and b. Profile D, $C_\alpha = 30$, $C_\omega = -100$. **a** E_0, $E_N = E_1 + E_2 + E_3$, E_2, E_3 as functions of time. **b** M and P as functions of time, and evolution in the M/P plane

studied the evolution of initial fields located at arbitrary points of the P/M diagram. We found a "critical" value of C_α, C_α^* say, that separated two types of behaviour: $C_\alpha^* \simeq 15$. For $C_\alpha \geq C_\alpha^*$, the situation is quite complex. There appears to be only one absolutely stable solution, a limit cycle with P near to -1. For the accessible range of C_α, this solution has small values of M; for example with $C_\alpha = 30$, $0.001 \lesssim M \lesssim 0.029$. The range of values of P and M in the oscillation increases slowly with C_α. For example at $C_\alpha = 50$, $-0.998 \lesssim P \lesssim 0.937$, $0.001 \lesssim M \lesssim 0.045$. The field is a combination of $m = 0, 1, 2, 3, \ldots$ modes, with the $m = 0$ dominating and the energy in the $m > 0$ modes decreasing rapidly as m increases. We reran this calculation with higher r, θ spatial resolution ($NI = 51$, $NJ = 101$), smaller time step ($\Delta\tau = 2.5\,10^{-5}$) and more azimuthal modes ($N = 5$); the solution was little changed. In Fig. 1 we display the energies in the $m = 0, 1, 2, 3$ modes and the variations of M and P as functions of time, and also the evolution of a typical solution towards the limit cycle. Figure 2 gives contours of constant surface field strength, and also field lines and toroidal field contours for the $m = 0$ component at arbitrary phase.

However there are other solutions (at $C_\alpha = 30$ at least) that are stable to some, but not all, perturbations. These are situated at the corners of the P/M diagram. There is a metastable solution (steady) of **A**1 type ($P = -1.0$) and $M = 1.0$. For small enough perturbations this solution is stable, but when perturbed by ca. 5% it evolves towards the stable limit cycle near $(-1.0, 0.0)$. There is also a limit cycle with $P = +1.0$, $0.001 \lesssim M \lesssim 0.022$ and a steady solution with $P = +1.0$, $M = 1.0$. These are both stable to $P = +1$ perturbations but not to those of odd parity. When the (1.0, 1.0) solution is disturbed, its initial evolution is particularly slow. Computations started from other points in the (P, M) plane all seem eventually to evolve towards the cycle with P near -1, M small, although the evolution is often so slow (timescale of tens of diffusion times) that it is impractical to follow it all the way to this stable solution. We did not find any stable solutions with large

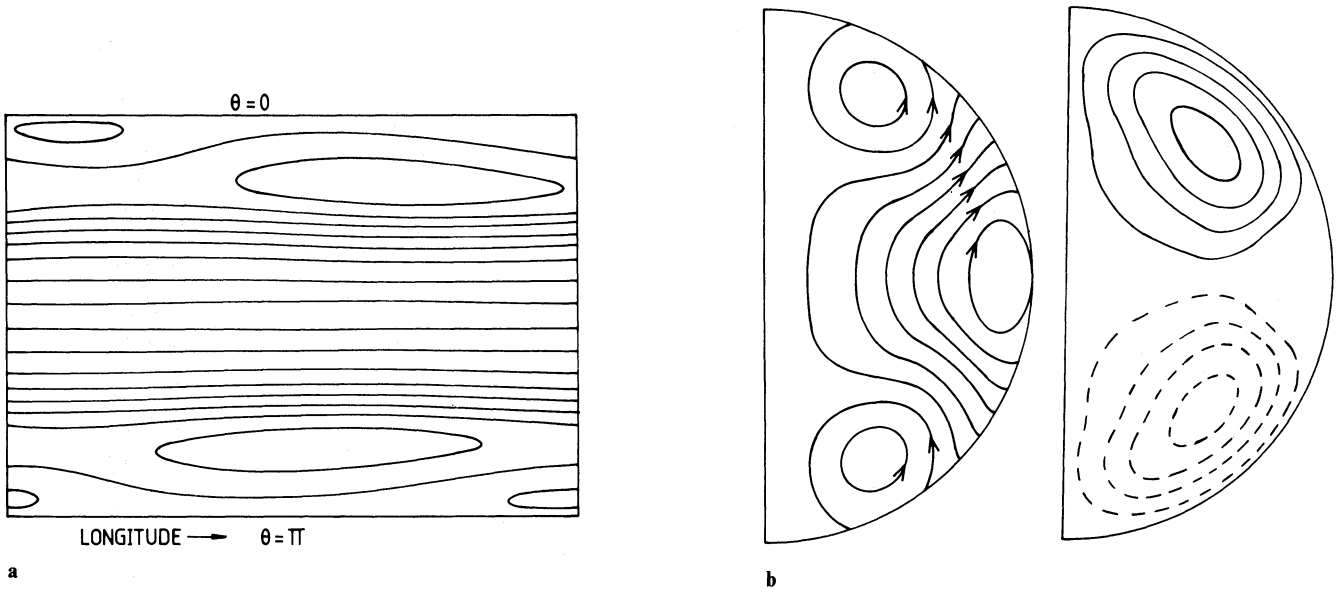

Fig. 2a and b. Profile D, $C_\alpha = 30$, $C_\omega = -100$. **a** Contours of constant surface field strength at $\tau = 2.5$. **b** Field lines and contours of constant toroidal field strength for $m = 0$ component at $\tau = 2.5$. Broken contours indicate negative values

Table 3

Profile	C_ω	C_α	(P, M)	Solution
D	-100	$< C_\alpha^*$	$(-1, 0)$	**A0**: limit cycle, stable
		$< C_\alpha^*$	(1, 1)	**S0**: limit cycle, unstable to nonaxisymmetric perturbations
		$> C_\alpha^*$	$(-0.9 \ldots$ to $-0.09 \ldots$, 0.001 to 0.03 $\ldots)$	Limit cycle, close to **A0**, stable[a]
		30	$(-1, 1)$	**A1**: steady, metastable
		30	(1, 0 to 0.02)	Limit cycle, close to **S0**, unstable to odd parity perturbations
		30	(1, 1)	**S1**: steady, unstable to odd perturbations
E	-150	≤ 20	(1, 1)	**S1**: steady, stable
	-300	$\lesssim 10$	(1, 1)	**S1**: steady, stable
		$\gtrsim 10$	$(-1, 0)$	**A0**: limit cycle, stable
	-350	5	$(-1, 0)$	**A0**: limit cycle, stable

[a] Except for perturbations large enough to bring the configuration into the basin of attraction of the **A1** metastable solution. Amplitude of variations in P and M increases with C_α

nonaxisymmetric parts in the range of C_α that we investigated ($C_\alpha \leq 30$ mostly, although we performed one calculation at higher resolution with $C_\alpha = 50$).

When $C_\alpha < C_\alpha^*$, the **A0** solution is a limit cycle that is stable to all perturbations. At $C_\alpha = 10$, the **S0** solution appears to be stable to nonaxisymmetric perturbations, but unstable to odd parity axisymmetric perturbations. The $P = M = 1$ solution is now unstable to small perturbations. We speculate that these results are typical for $C_\alpha < C_\alpha^*$. The various solutions are summarized in Table 3.

4.4. Profile E

The linear results presented in Table 1 led us to investigate two values of C_ω in some detail, although we did not investigate this profile as thoroughly as profile D. In particular we did not make the tests for metastability and for stability to a limited range of perturbations that are described in the previous section. A summary of the solutions found is given in Table 3.

4.4.1. $C_\omega = -150$

For all supercritical values of C_α that we studied (up to $C_\alpha = 20$), the only stable solution found is an entirely nonaxisymmetric steady solution of even parity (**S1**). In particular, the **A0** and **S0** modes are unstable to small nonaxisymmetric perturbations. Fig. 3 shows the variation of E_0, E_N, E_2, E_3, P and M with time and the evolution of a typical solution in the P/M plane. $E_N = E - E_0$ is the energy in the nonaxisymmetric field components. Figure 4 gives surface field strength contours.

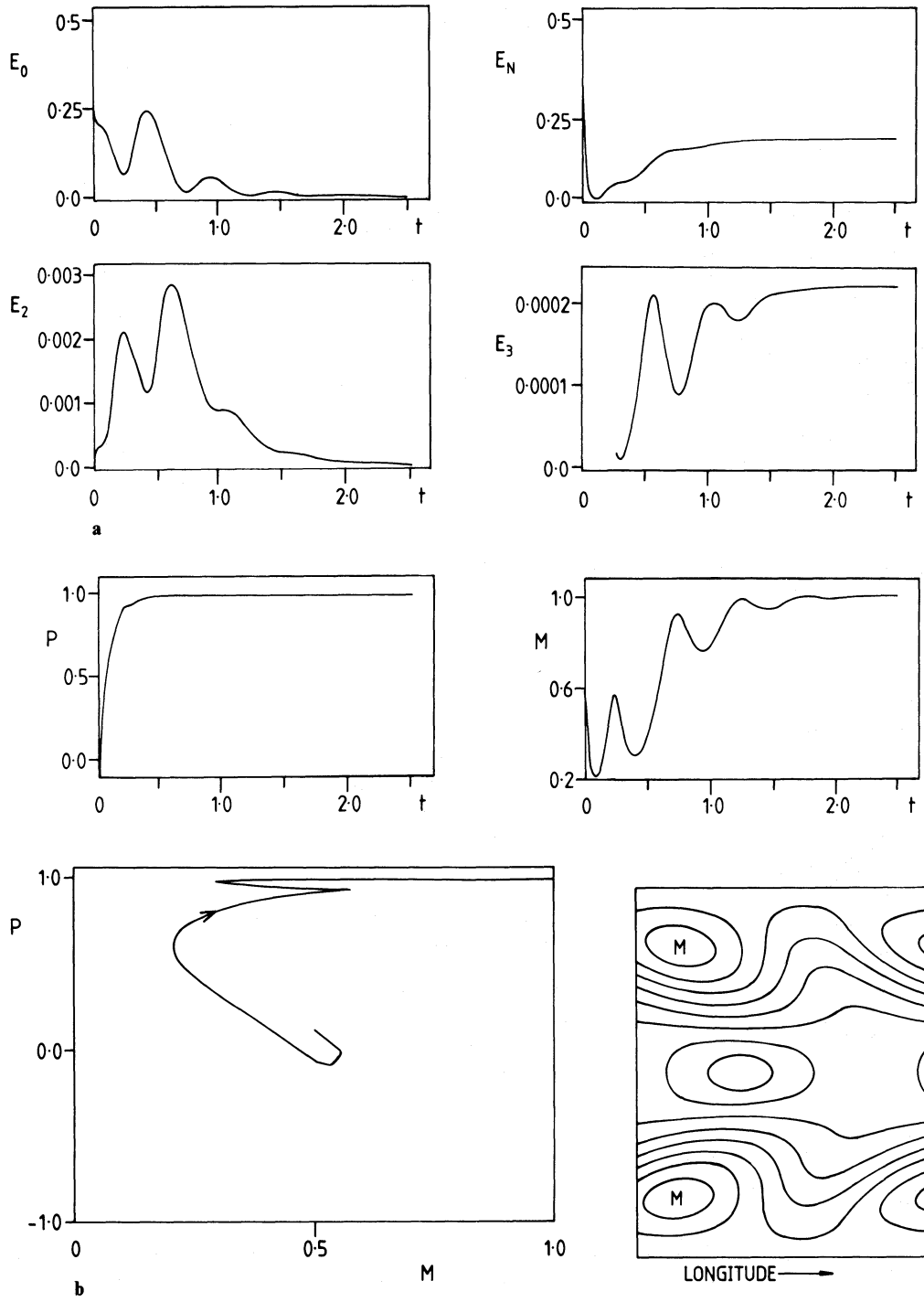

Fig. 3a and b. Profile E, $C_\alpha = 5$, $C_\omega = -150$. **a** E_0, E_N, E_2, E_3 as functions of time. **b** M and P as functions of time and evolution in the M/P plane

Fig. 4. Profile E, $C_\alpha = 5$, $C_\omega = -150$. Contours of constant surface field strength at $\tau = 2.5$. Regions of maximum field strength are indicated by 'M'

4.4.2. $C_\omega = -300$

In this case we discovered a value of C_α, say C_α^*, where $9.5 < C_\alpha^* < 10$, such that for supercritical $C_\alpha < C_\alpha^*$ the only stable solution found was the analogue of that described for the case $C_\omega = -150$, i.e. a purely nonaxisymmetric even parity (S1) steady solution. For $C_\alpha^* < C_\alpha \leq 20.0$ the only stable solution appears to be the A0 solution (limit cycle). Thus C_α^*, for this value of C_ω, marks a watershed between the existence of stable axisymmetric and stable nonaxisymmetric solutions.

4.4.3. Larger values of $|C_\omega|$

In the light of the results described above, and given our expectation that for large enough $|C_\omega|$ nonaxisymmetric modes

will be suppressed, we evolved fields from an initial configuration located near the middle of the P/M diagram with a slightly supercritical $C_\alpha = 5$ and with $C_\omega = -325$ and -350. When $C_\omega = -325$ the solution evolves to an even parity nonaxisymmetric steady configuration corresponding to that described above. With $C_\omega = -350$ the system eventually settles to an oscillatory A0 solution that appears to be the only stable configuration.

5. Discussion and conclusions

Our calculations reveal some of the wide variety of nonlinear behaviour that is possible for supercritical nonlinear mean field dynamos when the restriction to axisymmetry is dropped. The behaviour of the systems that we studied depends quite sensitively both on the assumed profiles of differential rotation and α-effect, and also on their magnitude via the parameters C_ω and C_α. In one example we find a "watershed" value of C_α separating regimes of stable axisymmetric and stable nonaxisymmetric solutions (profile E). With the same source profiles, but a different value of C_ω, only nonaxisymmetric solutions were stable in the accessible range of C_α. In contrast, with a slightly different distribution of angular velocity (profile D), there is a transition from a stable axisymmetric to a stable mixed ($m = 0, 1, 3, \ldots$) solution as C_α increases. The sensitivity of the detailed nature of the results to the differential rotation profile is additionally emphasized by preliminary results reported in Moss (1991), when x_ω takes values between 0.40 and 0.70, leaving the other parameters unaltered.

However we have not yet found a model in which the axisymmetric modes are very much more easily excited in linear theory but nonaxisymmetric field components persist in the nonlinear regime, but see profile D, Sect. 4.3.

We can note that the observations of HD32918 might suggest the presence of a predominantly S1 field, but it is obviously quite premature to attempt to make any comparisons between our very idealized solutions and the sparse, inferential observational evidence for large scale nonaxisymmetric stellar fields. We content ourselves with observing that it *is* possible for large scale nonaxisymmetric fields to be preferred, and that axisymmetric and nonaxisymmetric solutions *can* interact to give a stable cycle. Whether or not the necessary α and Ω – profiles can exist as a part of a globally self-consistent solution is a much deeper and more difficult question.

Our code is adaptable, and allows the investigation of other forms of parameterized nonlinearity, and could be modified to include "real" dynamics by solving simultaneously the Navier-Stokes equation. Restriction of the dynamo to a shell rather than a complete sphere may also influence the results. These are all areas for future work.

Acknowledgement. The work described in this paper was initiated during a visit to Helsinki by DM under the Royal Society–Academy of Finland Exchange Scheme.

References

Brandenburg A., Krause F., Meinel R., Moss D., Tuominen I., 1989a, A&A 213, 411

Brandenburg A., Moss D., Tuominen I., 1989b, Geophys. Astrophys. Fluid Dyn. 49, 129

Chandrasekhar S., 1961, Hydrodynamic and Hydromagnetic Stability, Clarendon Press, Oxford

Jetsu L., Huovelin J., Tuominen I., Vilhu O., Bopp B.W., Piirola V., 1990, A&A 236, 423

Moss D., 1991, in: "The Sun and Cool Stars: activity, magnetism, dynamos", IAU Colloquium 130, eds. I. Tuominen, D. Moss, G. Rüdiger, Springer, Heidelberg (in preparation)

Piskunov N.E., Tuominen I., Vilhu O., 1990, A&A 230, 363

Rädler K-H., Wiedemann E., Brandenburg A., Meinel R., Tuominen I., 1990, A&A 239, 413

Rüdiger G., 1973, Astron. Nachr. 294, 183

Stix M., 1971, A&A 13, 203